# Porosity Effects in Hydrogen Reduction of Iron Oxides

The rates of reduction of hematite to magnetite and of magnetite to iron in hydrogen/nitrogen/water vapor atmospheres were each studied with respect to variation in temperature, gas composition, and solid pore structure. It is shown that at temperatures below 350°C, the reactions are under chemical kinetic control, and diffusional limitations are negligible. The activation energies for the reduction of hematite to magnetite and of magnetite to iron were found to be 185 kJ/mol and 76.6 kJ/mol, respectively. Both reactions exhibit first-order behavior for hydrogen partial pressures less than 76 kPa. The conversion and rate data for each reaction were interpreted in terms of the random pore model of Bhatia and Perlmutter (1980), which takes into account the detailed pore structure of the starting material as well as the changes that occur as the reaction proceeds. The model predictions of conversion with time agree with the measured data to within 2%, and the rate vs. conversion predictions agree to within 5%.

**Arthur J. Fortini**
**Daniel D. Perlmutter**
Department of Chemical Engineering
University of Pennsylvania
Philadelphia, PA 19104

## Introduction

It has been known since the work of Tennenbaum and Joseph (1939) that the reduction of the several stable oxides of iron proceeds as a series of steps from one oxide to the next and finally to the metal. At temperatures low enough to suppress the formation of FeO, the reduction of iron oxide by hydrogen follows the two-step reaction sequence:

$$3Fe_2O_3 + H_2 \rightarrow 2Fe_3O_4 + H_2O; \quad \Delta H_r^1 = 27.8 \text{ kJ} \qquad (1)$$

and

$$Fe_3O_4 + 4H_2 \rightarrow 3Fe + 4H_2O; \quad \Delta H_r^2 = 170 \text{ kJ} \qquad (2)$$

Edstrom (1953), and Edstrom and Bitsianes (1955) studied the reduction of single crystals of hematite and magnetite to iron at temperatures ranging from 600 to 1,100°C. Optical microscopy of the samples after partial reduction at 1,000°C showed well defined interfaces among the various oxide phases. Srinivassan and Sheasby (1981) further studied the reduction of hematite to magnetite at temperatures between 700 and 900°C via scanning electron microscopy. They too reported well defined interfaces whose growth tended to preserve existing interface geometry even in the area surrounding a pore. The microscopy data demonstrated, in addition, that all the product phases can be porous.

Addressing this point, Warner (1964) showed that hematite samples reduced under identical atmospheres but at different temperatures yielded iron products with very different pore structures. Specifically, the high-temperature 950°C product contained larger, coarser pores than one reduced at the lower temperature of 750°C. This observation was confirmed by Turkdogan et al. (1971), who performed mercury penetration porosimetry experiments on the iron products. Their data indicate that, below 600°C, the mean pore radius in the iron is of the order of 100 Å.

Bradshaw and Matyas (1976) studied the reduction of hematite to magnetite in $CO/CO_2$ atmospheres and performed mercury porosimetry experiments on the product. Their data indicated that the size of the pores formed in the magnetite phase decreases with reduction temperature. For hematite reduced at 500°C, their data show a mean pore radius of 300 Å. Swann and Tighe (1977) also investigated the reduction of hematite to magnetite in $CO/CO_2$ atmospheres. Their SEM data show grain boundaries opening and forming pores in nonporous, polycrystalline hematite, producing a mean pore radius of approximately 80 Å for reduction at 400°C. Where authors have reported magnetite layers to be nonporous (Edstrom, 1953; St. John and Hayes, 1982; Srinivassan and Sheasby, 1981), the maximum resolution of their microscopy observations was approximately 0.5 to 1.1 micron, too large a dimension to detect any significant porosity in their samples.

In view of these findings, it is clear that interpretive models for the rates of reactions 1 and 2 must make allowance for the

porosities of both reactants and products. This is done in the analysis of the results to be reported here: the pore structures of the starting materials were measured, and the changes in the pore structure as the reactions proceeded were quantified. The rates were confined to the regime of chemical kinetic control for both the reduction of hematite to magnetite and of magnetite to iron, each in hydrogen/water vapor/nitrogen atmospheres. The reactions were each run at a temperature low enough to eliminate diffusional limitations.

## Background

### *Diffusional limitations*

Warner (1964) studied the reduction of large (1 cm diameter) hematite samples by hydrogen and water vapor and assumed that gaseous diffusion was the rate-determining step. He was able to calculate the effective binary diffusivities of hydrogen and water vapor through the product phases, and was able to extract a tortuosity factor, by comparing his results with previously published values of the diffusivity. Olsson and McKewan (1966, 1970) also measured the effective diffusivity of hydrogen and water vapor through pellets of iron formed by the reduction of hematite under various conditions. Using these data they were able to demonstrate that the rate behavior previously observed by McKewan (1958, 1960, 1961, 1962a, b, 1965a, b) was significantly influenced by diffusion of gases through the product layer. It appears that the rates measured earlier by Edmiston and Grace (1966) and by Quets et al. (1960, 1961) were also strongly influenced by diffusion.

With the recognition that diffusion could play a dominant role, Spitzer et al. (1966a, b) developed a generalized picture of reduction of a nonporous sphere of hematite. Their work represented a significant departure from the earlier work, because mass transport to and from the sample, diffusion of gases through the product layer, and chemical reaction are all taken into account. Their results showed that while diffusion of gases through the product layer can play a dominant role in determining the overall rate of the reaction, the effects of the other resistance are not necessarily negligible. Following Spitzer et al., Turkdogan and Vinters (1971, 1972), and Turkdogan et al. (1971) determined ranges of particle size and temperature needed to guarantee that the reduction was controlled by chemical kinetics.

### *Model development*

Although the excellent developments of Spitzer et al., Turkdogan and Vinters, and Turkdogan et al. emphasized that both diffusion and chemical kinetics can play an important role in determining overall rate behavior, their models are applicable only to the reduction of nonporous spheres of hematite, since they do not take into account the detailed pore structures or the exact surface areas of the solid reactants.

A general model for gas-solid reactions that does focus on the changing pore structure is the random pore model of Bhatia and Perlmutter (1980), which has been demonstrated to be widely applicable for interpreting a variety of noncatalytic systems (Bhatia and Perlmutter, 1980, 1981, 1983a, b). This model allows for a distribution of pore sizes in the starting material and incorporates the effects of pore overlap at higher levels of conversion. The effects of intraparticle diffusion and/or diffusion through a solid reaction product have been incorporated into the model. It also includes the effects of the external particle surface area on the rate of reaction; however, the effects of the latter are negligible for most applications.

The conversion vs. time and rate vs. conversion relationships for a reaction under kinetic control reduce to:

$$X = 1 - \exp\left[-\tau\left(1 + \frac{\psi\tau}{4}\right)\right] \tag{3}$$

$$\frac{dX}{d\tau} = (1 - X)\sqrt{1 - \psi \ln(1 - X)} \tag{4}$$

where $\tau$ is the dimensionless time given by

$$\tau = \frac{\mathcal{R}S}{1 - \epsilon} t = Rt \tag{5}$$

and $\psi$ is a pore structure parameter given by

$$\psi = \frac{4\pi L(1 - \epsilon)}{S^2} \tag{6}$$

For values of $\psi < 2$, the model predicts a monotonically decreasing reaction rate; and for $\psi = 1$, it yields virtually the same results as the grain model of Szekely and Evans (1970). For values of $\psi > 2$, however, a maximum in rate is predicted at an intermediate level of conversion.

## Experimental Procedures

Two groups of experiments were performed in this investigation. The first group used nitrogen gas adsorption to obtain values for the pore structure parameter, and the second set based on thermogravemetric analysis (TGA) generated conversion versus time data for each of the reduction reactions for comparison to the model predictions.

Samples of starting material were prepared by cold pressing 0.6 g of hematite powder in a 1 in. (25.4 mm) diameter die at 877 MPa for 120 seconds to form pellets of thickness 0.46 ± 0.03 mm (standard deviation). These samples had satisfactory handling properties, but were thin enough to make negligible any limitations due to diffusion. It was not found necessary to sinter the samples after preparation. Samples for porosity study of magnetite were prepared by reducing hematite pellets at 320°C in a flowing hydrogen/water vapor/nitrogen atmosphere. Each run required approximately 5 hours to reach 98% conversion. Additional samples of magnetite were obtained for kinetic studies by reducing the hematite pellets at 350°C in the same gaseous environment.

### *Pore structure*

Nitrogen adsorption was used to estimate the total pore volume, the pore surface area, and the pore length, the three parameters needed to evaluate $\psi$ via Eq. 6. The resulting cumulative pore volume as well as the pore volume distribution curve for an unreacted sample of hematite are shown in Figure 1, and the corresponding cumulative pore surface area is shown in Figure 2. Also superimposed on Figure 1 is the value of the total pore volume measured directly by desorption at a relative pressure close to unity. Similarly, Figure 2 also shows the total surface area as determined from the BET isotherm. The differences

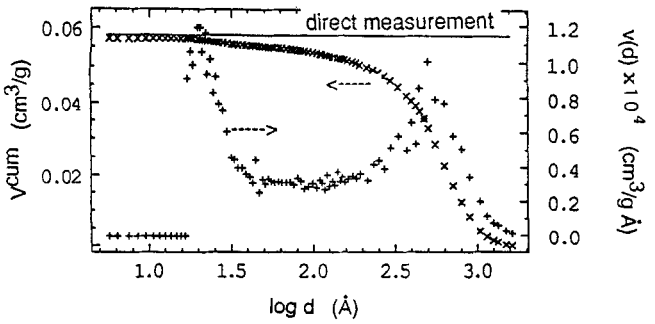


**Figure 1. Cumulative pore volume and pore volume distribution curves for hematite starting material.**
Curves based on nitrogen adsorption data

between the calculated values and the directly measured values is in both cases less than 1%, and this distribution curve was integrated to obtain the total pore length:

$$L = \int_0^\infty \frac{v(r)}{\pi r^2}\, dr \tag{7}$$

Nitrogen adsorption studies on the magnetite samples indicated a significant amount of microporosity, as shown in Table 1. Because this sample contains a significant amount of micropores, the Langmuir equation gives a better fit to the data than the BET equation (Lowell, 1979).

### *Thermogravimetric analysis*

The conversion vs. time data for the two reduction reactions were obtained by TGA, using a Cahn System 113 Electrobalance in a continuous flow system. The electrobalance is capable of measuring full-scale mass changes between 10 $\mu$g and 1 g with four digit accuracy. The furnace is equipped with a PID controller capable of maintaining the temperature to within +/ − 0.5°C. The gas supply system delivered specified flow rates of grade-5 hydrogen, grade-5 nitrogen, and water vapor (distilled and deoxygenated). A vacuum pump and a liquid nitrogen trap evacuated the system prior to each run.

To study the kinetics of the second reduction step, the magnetite was formed *in situ* by reducing hematite to magnetite under conditions identical to those used during the first reaction. The atmosphere for this first step was determined by selecting a value of $P_H$ and then operating with $P_H/P_w$ as close to 16.4 as possible. After the reduction to magnetite reached completion (typically in less than 20 min), the system was evacuated to remove all water vapor and it was rapidly filled with nitrogen, the sample was weighted, the proper hydrogen/nitrogen mixture was introduced, and the reaction was allowed to run.

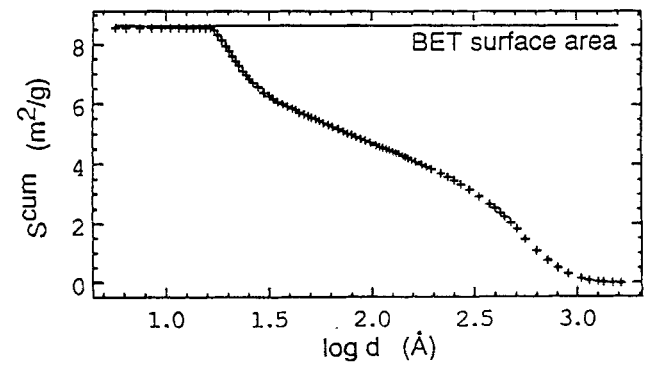


**Figure 2. Cumulative pore surface area curve for hematite starting material.**
Curve based on nitrogen adsorption data

**Table 1. Pore Characteristics of Solid Reactants**

| | Total Pore Surface m$^2$/g | Total Pore Volume cm$^3$/g |
|---|---|---|
| *Hematite (Starting Material)* | | |
| Mesopores from experimental distribution curve | 8.66 | 0.0574 |
| Mesopores plus micropores by BET | 8.64 | |
| Micropores after Lowell (1979) | None | None |
| Mesopores plus micropores by direct measurement | | 0.0581 |
| *Magnetite (from Partially Reduced Hematite)* | | |
| Mesopores from experimental distribution curve | 5.81 | 0.0382 |
| Mesopores plus micropores by BET | 8.10 | |
| Micropores after Lowell (1979) | 7.8 | 0.00174 |
| Mesopores plus micropores by direct measurement | | 0.0393 |
| Mesopores plus micropores after Langmiur and Lowell (1979) | 10.9 | |

## Results and Discussion

In considering the experimental results, it should first be noted that wustite (FeO) is thermodynamically unstable at temperatures below 560°C. To confirm this expectation X-ray diffractometry was performed on a sample of hematite which was partially reduced to iron to assure that wustite was not being formed during the low temperature reductions studied in this investigation. Further details and the X-Ray diffraction patterns may be found in Fortini (1988).

### *Effects of sintering*

In the absence of any sintering during the hematite to magnetite reduction, an increase in total pore volume of 2.23% would be expected from the respective molar volumes. Comparison of the data in Table 1 shows, however, that both the mesopore volume and the mesopore surface area decreased after reduction to magnetite, indicating that in fact some sintering did take place during the reduction. The micropore analyses were performed by the method described by Lowell (1979), indicating that no detectable micropores were present in the hematite startup material. Table 1 summarizes the results. The pore length distribution curve presented in Figure 3 was calculated from the pore volume distribution curve by using

$$l(d) = \frac{v(d)}{\pi r^2} \tag{8}$$

It is convenient to differentiate between the pores that were present in the starting material (Level-1) and the added pores that were formed by the reduction of the hematite to magnetite (Level-2): i.e., the Level-2 pores are the incremental pores and

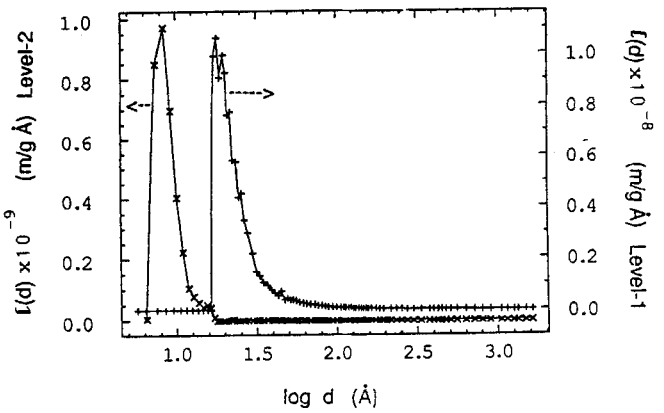


**Figure 3. Pore length distribution curves for level-1 and level-2 pores.**

do not include those initially present. In addition, a designation (Level-1,2) is needed to identify the overall structure of a sample containing both Level-1 and Level-2 pores. Accordingly,

$$\psi_{1,2} = \frac{4\pi(L_1 + L_2)(1 - \epsilon_1 - \epsilon_2)}{(S_1 + S_2)^2} \tag{9}$$

Two useful observations may be made with respect to the curves in Figure 3: 1) the two curves have the same shape, even though the distribution for the post-sintered material is shifted to smaller radii; and 2) the curves are free of any significant range of overlap. In effect, this means that the Level-1,2 distribution is the sum of the Level-1 and Level-2 curves, and further that all the pores have been similarly effected by the sintering process.

The foregoing description can be made quantitatively by assuming that all the pores decrease in radius by the same percentage during the sintering process, while no pores are completely destroyed: i.e., the total length of the Level-1 pores remains constant. Then the pore structure of the sample prior to sintering is given by

$$\int_0^\infty v_m(\alpha r)\, dr = 1.0223 \int_0^\infty v_h(r)\, dr \tag{10}$$

where $v_m$ and $v_h$ are the pore volume distribution curves for magnetite and hematite, respectively, and $\alpha$ is the multiplier by which each pore radius must be increased to produce results consistent with the expectation based on molar volumes. The computation yields $\alpha = 1.14$: i.e., each pore must increase in radius by 14% to compensate for the sintering effect. If $v_m(\alpha r)$ is the distribution curve of the magnetite prior to sintering, then the Level-2 pore structure can be determined by subtracting the pore length distribution of the Level-1 pores in the hematite from the pore length distribution determined from $v_m(\alpha r)$. The results are shown in Figure 3 and summarized in Table 2, together with computed values of $\psi_{1,2}$.

### *Controlling regimes*

Although the random pore model can also be applied to data that include the effects of diffusion, kinetic parameters are more precisely determined when diffusional limitations are negligible. In order to determine the conditions under which the reaction rates are controlled by chemical kinetics, each reduction step was studied at various temperatures with the reactant gas composition held constant. Since it was necessary to avoid iron formation at the high temperatures, the hydrogen to water molar ratio was kept below 16.5, as dictated by the equilibrium data shown in Figures 4 and 5. It was possible to measure the rate of the second reaction because the first reaction is much faster, and there is a distinct leveling-off in the conversion as the first reaction nears completion. The maximum reaction rates for each temperature are presented in Figures 6 and 7 on standard Arrhenius coordinates.

For the lower temperature reduction of hematite to magnetite, the data in Figure 6 show asymptotic behavior (chemical kinetics control) when $10^4/T > 15.5$, corresponding to temperatures less than about 372°C. The activation energy associated with this segment of the curve is 185 kJ/mol, a value comparable with the 188 kJ/mol activation energy reported by Turkdogan and Vinters (1972), but of course much larger than those typically reported in the studies that were strongly influenced by diffusion. The data for the reduction of magnetite to iron in Figure 7 show chemical-kinetics-controlling behavior for $10^4/T > 15.0$, corresponding to temperatures less than 394°C. The activation energy of this process is 76.6 kJ/mol in agreement with reported values (McKewan, 1961).

Another technique for determining whether or not a reaction is in the diffusion-limited regime is to compute the Thiele modulus:

$$\phi = \sqrt{\frac{a^2\rho(1 - \epsilon)}{vDM}\left(\frac{1}{C}\frac{dX}{dt}\right)} \tag{11}$$

The reaction rate term in parentheses is the observed rate, obtained directly from the experimental data. If the maximum rate is used, this will yield a "worst case" Thiele modulus which will indicate diffusional limitations before they actually become

**Table 2. Various Levels of Pore Structure**

| Material Treatment History | Level-1 Pores: Hematite Untreated (As Prepared) | Level-1, 2 Pores: Magnetite After Sintering (Measured) | Level-1, 2 Pores: Magnetite Prior to Sintering (Estimated) | Level-2 Pores: Magnetite Prior to Sintering (Estimated) |
|---|---|---|---|---|
| $V$ = Total pore volume, cm³/g | 0.0574 | 0.0454 | 0.0587 | 0.00978 |
| $S$ = Total pore surface, m²/g | 8.66 | 15.6 | 17.8 | 10.1 |
| $L$ = Total pore length, m/g | $4.84 \times 10^6$ | $3.86 \times 10^7$ | $3.86 \times 10^7$ | $3.29 \times 10^7$ |
| $\epsilon$ = Void fraction | 0.23 | 0.190 | 0.234 | 0.0482 |
| $\Psi$ = Pore structure parameter | 11.9 | 31.1 | 22.8 | 74.5 |

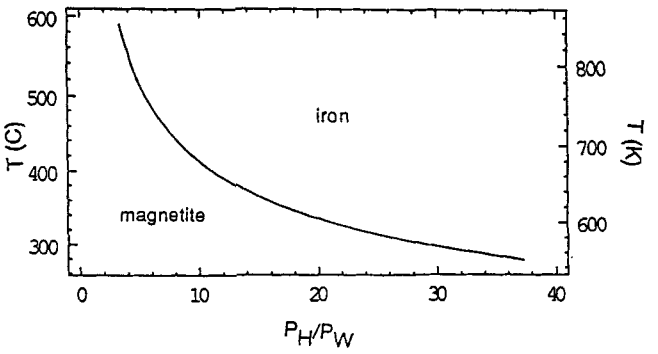


**Figure 4. Hydrogen to water vapor ratio for magnetite-iron equilibrium.**

important. For a reaction to be under kinetic control, the Thiele modulus must be appreciably less than unity. As can be seen from Figure 8, this is the case for both reactions for temperatures less than about 375°C, in agreement with the previous observations. On the basis of these findings, the reaction temperature was selected to be 350°C.

### *Thermal effects*

Since the two reduction reactions are endothermic with high values of activation energy, the influences of self cooling need to be estimated to assure that the reactions are effectively isothermal. For this purpose of transient heat balance gives

$$C_p(X)\frac{dT}{dt} = Ah(T_\infty - T_s) + AE\sigma(T_\infty^4 - T_s^4) - \Delta H\frac{dX}{dt}(X)\frac{\Delta m}{M} \quad (12)$$

where

$$C_p(X) = [1 - X]C_p^r + XC_p^p \quad (13)$$

Using the approximation $T_\infty^4 - T^4 \approx 4T^3(T_\infty - T)$, Eqs. 12 and 13 were solved with the initial condition $T = T_\infty$ and estimates for the pertinent parameters. The results indicate a maximum temperature drop of 0.12°C for the reduction of hematite and a drop of 0.57°C for the reduction of magnetite, corresponding to 0.7% and 1% decreases in the respective rates of reaction, insignificant compared to other uncertainties in the experimental data.

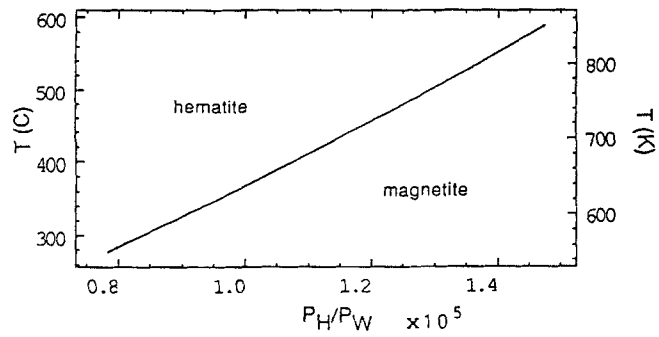


**Figure 5. Hydrogen to water vapor ratio for hematite-magnetite equilibrium.**

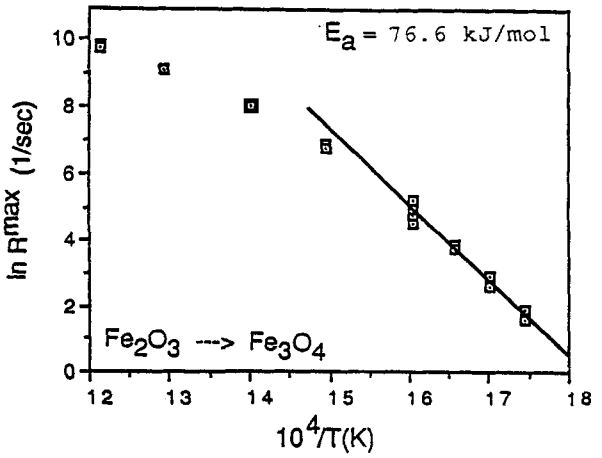


**Figure 6. Arrhenius plot for the reduction of hematite.**

### *Orders of reaction*

To assess the extent of reversibility to be expected from the hematite to magnetite reaction, data from the JANAF Thermochemical Tables (Stull and Prophet, 1970) were used to estimate an equilibrium constant from the reaction. The computed ratio of $(k_f/k_r) \approx 10^5$ indicates that the reaction is effectively irreversible under the conditions of this study. Assuming in accordance with the prior report of Srinivassan and Sheasby (1981) that the reaction is first-order:

$$R^{max} = k_f P_H \quad (14)$$

The isothermal reduction was carried out under atmospheres of hydrogen, water vapor, and nitrogen, varying the hydrogen to water vapor ratio from 3.0 to 15.6 and the partial pressure of hydrogen from 19 to 71 kPa. The results are shown in Figure 9 to demonstrate the agreement with the expected linearity to the origin.

The reduction of magnetite to iron is also reported (Al Kahtany and Rao, 1980; McKewan, 1962b) to be first-order with respect to hydrogen partial pressure. The data in Figure 4 indicate that the process can be treated as irreversible, only if hydrogen and nitrogen are present in the reactant gas stream. This

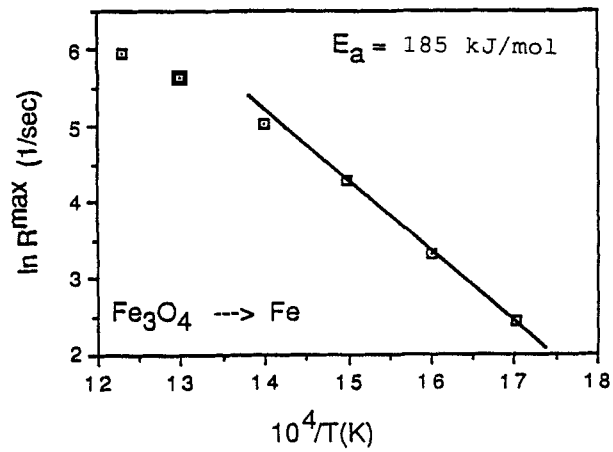


**Figure 7. Arrhenius plot for the reduction of magnetite.**

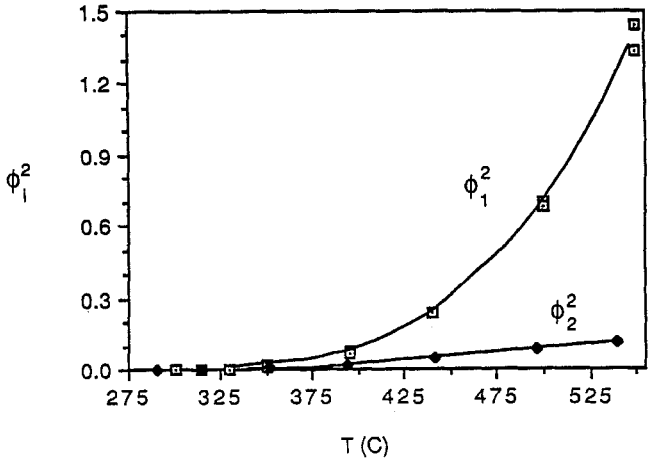


**Figure 8. Thiele modulus for each reduction reaction as a function of temperature.**

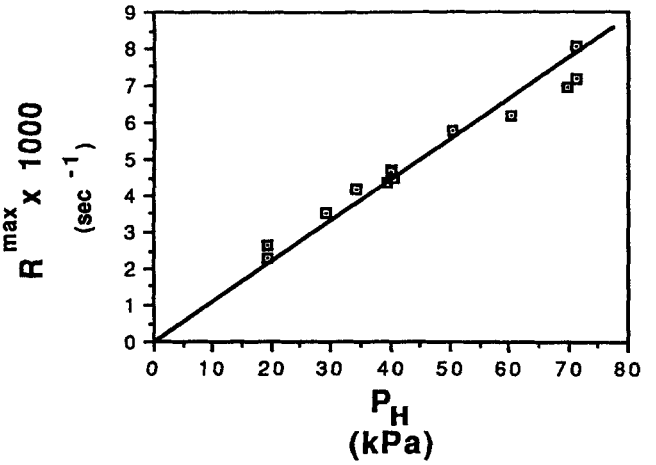


**Figure 9. Hematite to magnetite reduction data plotted as first order and irreversible.**

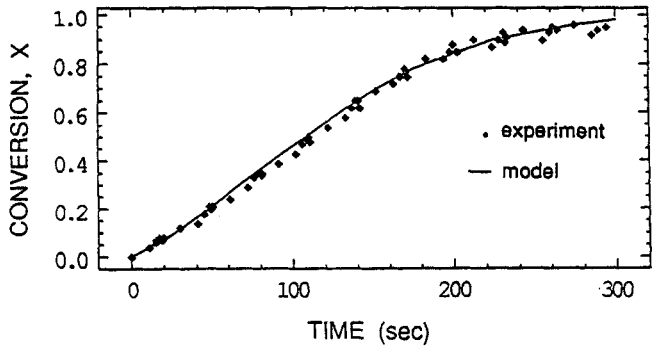


**Figure 10. Conversion v. time behavior for reduction of hematite to magnetite.**
$P_H$ = 0.47 kPa; $P_H/P_w$ = 15.3

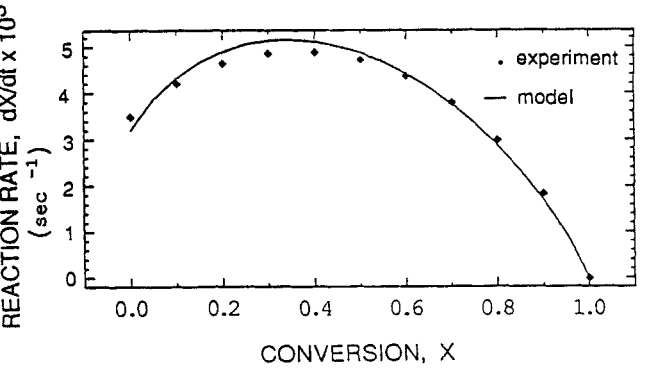


**Figure 11. Rate v. conversion behavior for reduction of hematite to magnetite.**
$P_H$ = 0.47 kPa; $P_H/P_W$ = 15.3

was effected in this study by using a large excess of reactant gas (100:1) and high flow rates (12 cm/s) in the reactor.

### *Modeling the reaction rates*

To test the agreement between the random pore model and experiments, measured kinetic data were fit to Eq. 3 using both $R$ and $\psi$ as fitting parameters. The resulting least squares value of $\psi$ was then compared to that obtained from the initial pore structure measurements via Eq. 6. For the first reaction the two determinations of $\psi$ agreed to within 1.7%, corresponding to a spread of only 1.2% for $R_1^1$. By combining this value of $R_1^1$ with the porosity and surface area measurements in Table 2, Eq. 5 yields $\mathcal{R}_1 = 5.42 \times 10^{-9}$ cm/s, which is the rate at which the reaction interface moves through the solid hematite.

Figure 10 shows the predicted conversion versus time data using $\psi_1 = 11.9$ and $R_1^1 = 3.20 \times 10^{-3}$/s in Eq. 3. The experimental data from several replicate runs are superimposed and show the model to agree to within the experimental error in the measured data—about 0.04 conversion units. Figure 11 shows the rate vs. conversion predictions using the same parameter values and Eq. 4. Again, the agreement between the model and the fitted data is everywhere within 5%.

To test the agreement between model and experiment for the reduction of magnetite to iron, conversion versus time data were again fit to Eq. 3 using $R_2^{12}$ and $\psi_{1,2}$ as fitting parameters, where the subscript, 1,2 indicates that both Level-1 and Level-2 pores are present in the magnetite. As was done in the previous case,

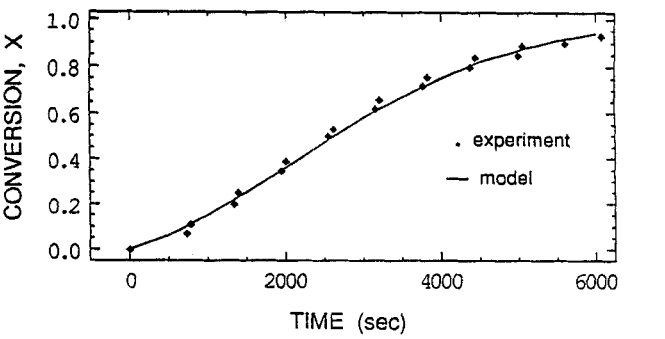


**Figure 12. Conversion versus time behavior for reduction of magnetite to iron.**
$P$ = 0.47 kPa; $P$ = 0.0 kPa

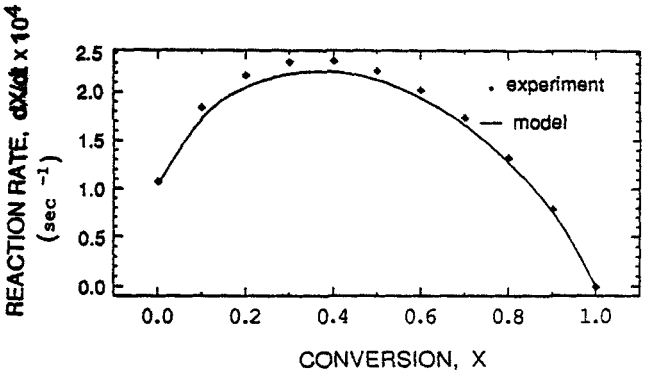


**Figure 13. Rate v. conversion behavior for reduction of magnetite to iron.**
$P_H$ = 0.47 kPa; $P_W$ = 0.0 kPa

the resulting value of $\psi_{1,2}$ was compared to the value obtained by porosimetry experiments. The agreement between the two estimates of $\psi_{1,2}$ is within 3%, corresponding to 2% between the two estimates of $R_2^{12}$. By combining the value of $R_1^{12}$ with porosity and pore surface area measurements via Eq. 5, one obtains $\mathcal{R}_2 = 8.65 \times 10^{-11}$ cm/s. Figure 12 shows the experimental data from several runs and the predicted conversion versus time behavior of the system using $\psi_{1,2} = 22.8$ and $R_2^{12} = 1.04 \times 10^{-4}$ $s^{-1}$. Figure 13 shows the rate versus conversion predictions using the same parameter values. Figures 12 and 13 show agreement between theory and experiment to within 4% and 7%, respectively.

## Notation

$a$ = half thickness of pellet
$A$ = geometric surface area of pellet
$C$ = vapor phase concentration of hydrogen
$C_p p$ = heat capacity of product phase
$C_p^r$ = heat capacity of reactant phase
$D$ = effective diffusivity of hydrogen through pellet
$d$ = pore diameter
$E$ = emissivity
$h$ = heat transfer coefficient
$\Delta H$ = heat of reduction reaction
$k_f$ = forward reaction rate constant
$k_r$ = reverse reaction rate constant
$l(d)$ = pore length distribution function
$L$ = initial total pore length, $cm/cm^3$
$Dm$ = mass change associated with reduction reaction
$M$ = molecular weight
$P_H$ = partial pressure of hydrogen
$P_W$ = partial pressure of water vapor
$r$ = pore radius
$R_i j$ = reaction rate of reaction $i$ occurring in level $j$ pores, 1/s
$R^{max}$ = maximum observed reaction rate, 1/s
$\mathcal{R}_i$ = rate of reaction $i$ interface movement, cm/s
$S$ = initial total pore surface area, $cm_2/cm_3$
$t$ = time
$T_s$ = temperature of sample, K
$T_\infty$ = temperature of environment surrounding sample
$v_h(d)$ = pore volume distribution function of hematite
$v_m(d)$ = pore volume distribution function of magnetite
$X$ = fractional conversion

### *Greek letters*

$\alpha$ = multiplier defined by Eq. 10
$\epsilon$ = initial porosity of sample
$\nu$ = ratio of stoichiometric coefficients
$\rho$ = density, $g/cm^3$
$\sigma$ = Stephan Boltzman constant
$\tau$ = dimensionless time defined in Eq. 5
$\phi$ = Thiele modulus
$\psi$ = pore structure parameter defined in Eq. 6

## Literature Cited


Al-Kahtany, M. M., and Y. K. Rao, "Reduction of Magnetite with Hydrogen: Part 1 Intrinsic Kinetics," *Ironmaking and Steelmaking*, **2**, 29 (1980).

Bessieres, A., J. Bessieres, and J. J. Heizmann, "Etude des Reactions Doubles Simultanees lors de la Reduction des Oxydes de Fer," *Rev. Metall.*, **75**(1), 13 (1978).

Bessieres, A., J. J. Heizmann, J. Bessieres, and R. Baro, "Contribution a l'Etude Cinetique de la Reduction de la Magnetite $Fe_3O_4$ en Wustite $Fe_{1-x}O$ par l' Oxyde de Carbone," *Rev. Metall.*, **73**(1), 179 (1976).

———, "Eude de la Cinetique de Reduction de $Fe_3O_4$-en $Fe_{1-x}O$: II. Etude du Regime Mixte," *Rev. Metall.*, **74**(1), 3 (1977).

Bhatia, S. K., and D. D. Perlmutter, "A Population Balance Approach to the Modeling of Solid Phase Reactions," *AIChE J.*, **25**, 298 (1979).

———, "A Random Pore Model for Fluid-Solid Reactions: I. Isothermal, Kinetic Control," *AIChE J.*, **26**, 379 (1980).

———, "A Random Pore Model for Fluid Solid Reactions: II. Diffusion and Transport Effects," *AIChE J.*, **27**, 247 (1981).

———, "Effect of the Product Layer on the Kinetics of the $CO_2$-Lime Reaction," *AIChE J.*, **29**, 79 (1983a).

———, "Unified Treatment of Structural Effects in Fluid-Solid Reaction," *AIChE J.*, **29**, 281 (1983b).

Bradshaw, A. V., and A. G. Matyas, "Structural Changes and Kinetics in the Reduction of Hematite," *Met. Trans. B*, **7B**, 81 (1976).

Edmiston, W. A., and R. E. Grace, "Kinetics of Near-Equilibrium reduction of Wustite," *Trans. AIME*, **236**, 1547 (1966).

Edstrom, J. O., "The Mechanism of the Reduction of Iron Oxides," *J. Iron and Steel Inst.* **175**, 289 (1953).

Edstrom, J. O., and G. Bitsianes, "Solid State Diffusion in the Reduction of Magnetite," *Trans. AIME*, **200**, 760 (1955).

Fortini, A. J., "Hydrogen Reduction of Iron Oxides," PhD Diss., Univ. of Pennsylvania, Philadelphia (1988).

Lowell, S., *Introduction to Powder Surface Area*, Wiley, New York (1979).

McKewan, W. M., "Kinetics of Iron Ore Reduction," *Trans. AIME*, **212**, 791, (1958).

———, "Kinetics of Iron Ore Reduction," *Trans. AIME*, **218**, 2 (1960).

———, "Reduction Kinetics of Magnetite in $H_2$-$H_2O$-$N_2$ Mixtures," *Trans. AIME*, **212**, 791 (1958).

———, "Reduction Kinetics of Hematite in Hydrogen-Water Vapor-Nitrogen Mixtures," *Trans. AIME*, **224**, 2 (1962a).

———, "Reduction Kinetics of Hematite in Hydrogen at High Pressure," *Trans. AIME*, **224**, 387 (1962b).

———, *Steelmaking: The Chipman Conference*, J. F. Elliott, ed., 141, The MIT Press, Cambridge, MA (1965a).

———, *Reactivity of Solids*, G. M. Schwab, ed., Elsevier, Amsterdam (1965b).

Olsson, R. G., and W. M. McKewan, "Diffusion of $H_2$-$H_2O$ Through Porous Iron Formed by the Reduction of Iron Oxides," *Met. Trans.*, **1**, 507 (1970).

Quets, J. M., M. E. Wadsworth, and J. R. Lewis, "Kinetics of Hydrogen Reduction of Magnetite," *Trans. AIME*, **218**, 545 (1960).

———, "Kinetics of Hydrogen Reduction of Magnetite to Iron and Wustite in Hydrogen-Water Vapor Mixtures," *Trans. AIME*, **221**, 1186 (1961).

St. John, D. H., and P. C. Hayes, "Microstructural Features Produced by the Reduction of Wustite in $H_2/H_2O$ Gas Mixtures," *Met Trans. B*, **13B**, 117 (1982).

Spitzer, R. H., F. S. Manning, and W. O. Philbrook, "Mixed-Control Reaction Kinetic in the Gaseous Reduction of Hematite," *Trans. AIME*, **236**, 726 (1966a).

———, "Generalized Model for the Gaseous, Topochemical Reduction of Porous Hematite Spheres," *Trans. AIME*, **236**, 1715 (1966b).

Srinivassen, M. V., and J. S. Sheasby, "A Study of the Reduction of Hematite to Magnetite Using a Stabilized Zirconia Cell," *Met. Trans. B*, **12B**, 177 (1981).

Stull, D. R., and G. Prophet, *JANAF Thermochemical Tables,* Office of Standard Reference Data, National Bureau of Standards, Washington, DC (1970).
Swann, P. R., and N. J. Tighe, "High Voltage Microscopy of the Reduction of Hematite to Iron," *Met. Trans. B,* **8B,** 479 (1977).
Szekely, J., and J. W. Evans, "A Structural Model for Gas-Solid Reactions with a Moving Boundary," *Chem. Eng. Sci.,* **25,** 1091 (1970).
Tennenbaum, M., and T. L. Joseph, "Reduction of Iron Ores under Pressure by Hydrogen," *Trans. AIME,* **135,** 59 (1939).
Turkdogan, E. T., R. G. Olsson, and J. V. Vinters, "Gaseous Reduction of Iron Oxides: Part II. Pore Characteristics of Iron reduced from Hematite in Hydrogen," *Met. Trans.,* **2,** 3189 (1971).
Turkdogan, E. T., and J. V. Vinters, "Gaseous Reduction of Iron Oxides: Part III. Reduction-Oxidation of Porous and Dense Iron Oxides and Iron," *Met. Trans.,* **3,** 1561 (1972).
Warner, N. A., "Reduction Kinetics of Hematite and the Influence of Gaseous Diffusion," *Trans. AIME,* **230,** 163 (1964).

*Manuscript received Oct. 5, 1988, and revision received Mar. 28, 1989.*